

Transfer of Fisher information in quantum postselection metrology

Zi-Rui Zhong(钟子瑞), Ke-Xuan Chen(陈可轩), Xia-Lin Su(苏夏临), Hui-Lin Xu(徐惠林), Yan Zhang(张妍), Xiang-Ming Hu(胡响明), and Qing-Lin Wu(吴青林)
Citation: Chin. Phys. B, 2026, 35 (**7**): 074203. DOI: 10.1088/1674-1056/ae194f
http://cpb.iphy.ac.cn; http://iopscience.iop.org/cpb

What follows is a list of articles you may be interested in

Design of a tunable Airy zoom metasurface based on the moiré effect

Baibing Li(李白冰), Jiatong Liu(刘家同), Hao Huang(黄浩), and Ruiting Hao(郝瑞亭)
Chin. Phys. B, 2026, 35 (**6**): 064211. DOI: 10.1088/1674-1056/ae5592

Resonance-enhanced high-harmonic generation and attosecond transient absorption spectroscopy of hydrogen atoms

Yue Cao(曹玥), Zheng Shu(舒正), Da-Wei Tian(田大纬), and Xiao-Lei Hao(郝小雷)
Chin. Phys. B, 2026, 35 (**6**): 064210. DOI: 10.1088/1674-1056/ae64cd

Photogalvanic effects in surface states of topological insulators under perpendicular magnetic fields

Haoyu Li(李浩宇), Kainan Chang(常凯楠), Wang-Kong Tse, and Jin Luo Cheng(程晋罗)
Chin. Phys. B, 2026, 35 (**5**): 054203. DOI: 10.1088/1674-1056/ae4c68

Supersymmetry-driven segmented tapered laser for stabilized single transverse and longitudinal mode engineering

Yiwen Lou(楼亦文), Tian Lan(兰天), Jun Qi(齐军), Jinlong Zhao(赵金龙), Ying Li(李颖), Baiyi Qin(覃柏颐), Yuying Liu(刘豫颖), Xuesheng Liu(刘学胜), and Zhiyong Wang (王智勇)
Chin. Phys. B, 2026, 35 (**4**): 044207. DOI: 10.1088/1674-1056/ae29f9

Bistable Goos-Hänchen shift owing to leaky-mode excitation in a slab waveguide with Kerr nonlinear medium

Yuan-Ping Cai(蔡园平), Li Jiang(姜丽), and Ren-Gang Wan(万仁刚)
Chin. Phys. B, 2026, 35 (**4**): 044203. DOI: 10.1088/1674-1056/ae00b3

Transfer of Fisher information in quantum postselection metrology

Zi-Rui Zhong(钟子瑞), Ke-Xuan Chen(陈可轩), Xia-Lin Su(苏夏临), Hui-Lin Xu(徐惠林), Yan Zhang(张妍), Xiang-Ming Hu(胡响明), and Qing-Lin Wu(吴青林)†

Department of Physics, Central China Normal University, Wuhan 430079, *China*

(Received 9 August 2025; revised manuscript received 28 October 2025; accepted manuscript online 30 October 2025)

Postselected weak measurement has shown significant potential for detecting small physical effects due to its unique weak-value-amplification phenomenon. Previous works suggest that Heisenberg-limit precision can be attained using optical coherent states. However, the observed Heisenberg scaling requires a measurement of the distribution of postselection probability, exhibiting no implementation pathway through conventional measurement paradigms. Here, we demonstrate that the output photons can also reach the Heisenberg scale by utilizing the Fisher information transfer effect, while this scenario exhibits enhanced robustness against dephasing noise. In addition, we consider the insertion of a power-recycling cavity and demonstrate its positive impact on the distribution of postselection. Our results enhance the quantum metrological advantages of the postselection strategy and broaden its application scope.

Keywords: optics, weak value, robustness

PACS: 42.50.Xa, 03.65.Ta, 06.30.Gv

DOI: 10.1088/1674-1056/ae194f **CSTR:** 32038.14.CPB.ae194f

1. Introduction

Postselected weak measurement, first introduced by Aharonov, Albert, and Vaidman in 1988,[1] has demonstrated rich potential in quantum mechanics, particularly in the area of parameter estimation and quantum measurement theory. It involves weak coupling between the system and the meter, enabling the average shift of the output pointer state to significantly exceed the eigenvalues of the system observable through postselection.[2] Generally, the amplification of the shift observable is associated with the concept of the 'weak value', a phenomenon known as the weak-value amplification (WVA) effect. With these characteristics, postselected weak measurement has been successfully used in the detection of tiny physical effects.[3–21]

The accuracy of a measurement is a crucial factor in assessing the effectiveness of a measurement method. Whether postselected weak measurement is optimal remains a point of significant debate.[22–35] Critics often address this issue from the perspective of Fisher information (FI), arguing that postselection, in itself, cannot improve accuracy and instead discards a significant portion of the photons that carry useful information.[29] Positive discussions focus on specific conditions. For example, weak measurement can outperform conventional measurement in the presence of detector saturation.[36,37] Additionally, weak measurement has been pointed out to suppress technical noise in some circumstances.[23,24,31,38–41] Some recent studies on WVA-based metrology include Refs. [42,43].

Since debates on weak measurement often center around low postselection efficiency, several targeted efforts have been made to address this issue. Recycling techniques have been demonstrated to enhance both the postselection probability and signal-to-noise ratio by reusing the failed postselection photons.[44–50] Additionally, joint weak measurement has been shown to maximize photon utilization and remain robust against various sources of noise.[51] Furthermore, certain quantum resources, such as entanglement and squeezing, can enhance the precision of WVA measurements to the quantum scale.[41,52–54] Some schemes even claim to achieve Heisenberg-scaling (HS) precision without relying on entanglement[55] or any quantum resources.[27,28,56,57] These works undoubtedly provide a broader perspective of the quantum potential of WVA-based metrology.

In this article, we focus on the WVA setup presented in Ref. [27], where the distribution of postselection can yield quantum-enhanced precision. We will demonstrate that the successful or failed post-selection states can also reach the quantum scale, utilizing the concentration or transfer effect of FI in weak measurement. In addition, we will show that recycling techniques can enable the post-selection process itself to benefit, rather than just the successful post-selection photons.

2. Model of coherent-state-assisted postselection measurement

In this section, we review the WVA-based setup introduced by Zhang *et al.*[27] The quantum system is a two-state system with eigenstates $|e\rangle$ and $|g\rangle$, which is coupled to an optical meter prepared in a coherent state $|\alpha\rangle$. The initial state of the quantum system is prepared as $|\psi_i\rangle = \cos(\theta_i/2)|g\rangle +$

†Corresponding author. E-mail: qlwu@ccnu.edu.cn

© 2026 Chinese Physical Society and IOP Publishing Ltd. All rights, including for text and data mining, AI training, and similar technologies, are reserved.

$\sin(\theta_i/2)\,e^{i\phi_i}|e\rangle$. The interaction Hamiltonian produces a unitary operation represented as follows:

$$U = \exp(ig\hat{\sigma}_z\hat{n}), \tag{1}$$

where g is the coupling parameter, $\hat{\sigma}_z$ is the Pauli operator $\hat{\sigma}_z = |e\rangle\langle e| - |g\rangle\langle g|$, and $\hat{n}$ is the photon-number operator $\hat{n} = \hat{a}^\dagger\hat{a}$. This results in the joint state being

$$\begin{aligned}|\Psi_j\rangle &= U|\psi_i\rangle|\alpha\rangle \\ &= \cos\frac{\theta_i}{2}|g\rangle|\alpha e^{-ig}\rangle + \sin\frac{\theta_i}{2}e^{i\phi_i}|e\rangle|\alpha e^{ig}\rangle.\end{aligned} \tag{2}$$

Postselecting the system in the state $|\psi_f\rangle = \cos(\theta_f/2)|g\rangle + \sin(\theta_f/2)\,e^{i\phi_f}|e\rangle$, the meter state becomes

$$|\widetilde{\Phi}_d\rangle = \cos\frac{\theta_i}{2}\cos\frac{\theta_f}{2}|\alpha e^{-ig}\rangle + \sin\frac{\theta_i}{2}\sin\frac{\theta_f}{2}e^{i\phi_0}|\alpha e^{ig}\rangle, \tag{3}$$

where $\phi_0 = \phi_i - \phi_f$ denotes the phase shift between the initial system state and the postselected system state. Notably, $|\widetilde{\Phi}_d\rangle$ is not normalized. The related normalized form should be $|\Phi_d\rangle = |\widetilde{\Phi}_d\rangle/\sqrt{P_d}$, where the normalization factors are given by $P_d = \langle\widetilde{\Phi}_d|\widetilde{\Phi}_d\rangle$, which is also the probability of successful postselection. Similarly, the failed postselected state can be written as $|\psi_r\rangle = \sin(\theta_f/2)|g\rangle - \cos(\theta_f/2)\,e^{i\phi_f}|e\rangle$, corresponding to the reflected probe

$$|\widetilde{\Phi}_r\rangle = \cos\frac{\theta_i}{2}\cos\frac{\theta_f}{2}|\alpha e^{-ig}\rangle - \sin\frac{\theta_i}{2}\sin\frac{\theta_f}{2}e^{i\phi_0}|\alpha e^{ig}\rangle. \tag{4}$$

Thus, the corresponding normalized forms are $|\Phi_r\rangle = |\widetilde{\Phi}_r\rangle/\sqrt{P_r}$, where $P_r = \langle\widetilde{\Phi}_r|\widetilde{\Phi}_r\rangle$ is the probability of failed postselection.

The FI is a central quantity in parameter estimation, denoted by F in this article. It establishes a lower bound on the variance of an unbiased estimator g through the Cramér–Rao inequality: $\mathrm{Var}(g) \geq 1/nF$. For a given probability distribution p_m, we can calculate the FI via the formula

$$F = \sum_m \frac{1}{p_m}\left(\frac{\mathrm{d}p_m}{\mathrm{d}g}\right)^2. \tag{5}$$

The quantum Fisher information (QFI) is defined as the FI maximized over all possible generalized measurements. When the meter function $|\Phi\rangle$ is known, the QFI can be calculated using the following formula:

$$Q = 4\left[\left(\frac{\mathrm{d}\langle\Phi|}{\mathrm{d}g}\right)\left(\frac{\mathrm{d}|\Phi\rangle}{\mathrm{d}g}\right) - \left|\langle\Phi|\left(\frac{\mathrm{d}|\Phi\rangle}{\mathrm{d}g}\right)\right|^2\right]. \tag{6}$$

By substituting $|\Phi_d\rangle$ and $|\Phi_r\rangle$ into Eq. (6), we obtain the QFI of the successful and failed postselection parts, denoted as Q_d and Q_r, respectively. $P_dQ_d + P_rQ_r$ stands for the maximum information from detecting photons. Besides, the distribution $\{P_d, P_r\}$ yields a classical FI F_p, which refers to the information obtained in the postselection process. Therefore, the total information contained at different stages of the selection-coupling-selection process is

$$F_{\mathrm{tot}} = P_dQ_d + P_rQ_r + F_p, \tag{7}$$

which is also one of the major conclusions of Ref. [27].

Next, we will demonstrate how to achieve the maximum F_{tot}. Notably, F_{tot} cannot exceed the input FI Q_j, which can be obtained by substituting $|\Psi_j\rangle$ into Eq. (6). It can be calculated that $Q_j = 4n^2\sin^2\theta_i + 4n$, where $n = |\alpha|^2$ is the average photon number. This expression suggests that $\theta_i = \pi/2$ can provide the maximum value

$$Q_j = 4n^2 + 4n, \tag{8}$$

where the upper limit of F_{tot} also reaches its maximum. Next, we examine the optimal region of F_{tot}. As shown in Fig. 1, we plot F_{tot}, P_dQ_d, P_rQ_r, and F_p varying with θ_f, where we set $n = 4$ and $\phi_0 = \pi$. We can clearly see that the peak F_{tot} corresponds to $\theta_f = \pi/2$ or $3\pi/2$ (considering only within one cycle), and the FI is concentrated in the postselection distribution. In this way, both Q_j and the maximum F_{tot} can exhibit quantum scaling ($\sim n^2$).

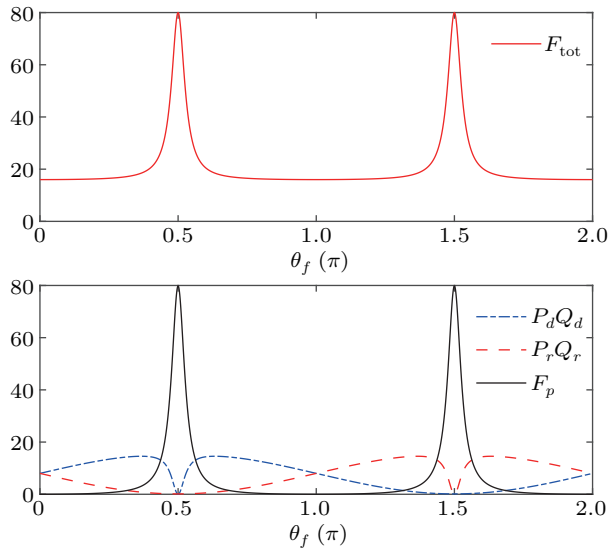


Fig. 1. FI Composition. Panel (a) corresponds to the cases of the total FI F_{tot} varying with θ_f. Panel (b) corresponds to the cases of the separated FI P_dQ_d, P_rQ_r and F_p varying with θ_f. In these plots, the average photon number is set to $\bar{n} = 4$. F_{tot} is the sum total of the FI contained at different stages of the preselection–coupling–postselection process. P_dQ_d is the QFI of successful postselection photons. P_rQ_r is the QFI of failed postselection photons. F_p is the FI of the distribution of postselection probability.

However, the quantum scale only occurs in the classical FI of the postselected process under the parameter conditions specified in previous literatures [27,28,30,56]. In other words, we need to establish a measurement scheme based on the postselection distribution rather than directly detecting the output state. This raises an immediate question: can the output meter state (P_dQ_d) reach the quantum scale?

3. The quantum perspective of P_dQ_d measurement

3.1. The information transfer effect

To begin with, we must reiterate the concept of a weak value,[1] which is typically employed to amplify measured parameters. Its mathematical form here is

$$A_{\rm w}=\frac{\langle\psi_f|\hat{\sigma}_z|\psi_i\rangle}{\langle\psi_f|\psi_i\rangle}=\frac{\sin\theta_i\sin\theta_f\,{\rm e}^{{\rm i}\phi_0}-\cos\theta_i\cos\theta_f}{\sin\theta_i\sin\theta_f\,{\rm e}^{{\rm i}\phi_0}+\cos\theta_i\cos\theta_f}. \quad (9)$$

Previous related works conclude that weak-value measurements can concentrate the input FI regarding the measured parameter into a small number of successful postselection events.[24,44,52] However, in Ref. [27], the FI is concentrated in the postselection distribution rather than in the typical aggregation of successful-postselection photons. This change stems from an alteration in the parameter region. For example, by focusing on one of the maximum $F_{\rm tot}$ parameter conditions where $\theta_i=\theta_f=\pi/2$, we can readily calculate that $A_{\rm w}=1$. However, this does not represent a strict weak-value measurement because there is no manifestation of the weak-value amplification effect. Reference [28] provides a more in-depth explanation of this issue; here, we merely emphasize that this measurement method is distinct from traditional weak-value measurement.

Next, we will demonstrate how this distinction significantly influences the postselection. The values of θ_i and θ_f are chosen to be $\pi/2$, which corresponds to the parameter condition for the maximum $F_{\rm tot}$ (this condition will be consistently applied in the following sections), and present the equation for the probability of successful postselection:

$$P_d=\frac{1+{\rm e}^{-2n\sin^2 g}\cos\left(n\sin 2g+\phi_0\right)}{2}. \quad (10)$$

When we apply the parameter settings from Ref. [27], where $\phi_0=\pi$ and a constant incident photon number, the postselection is introduced solely by the weak coupling g. However, for typical weak-value measurements, where the angle between the pre- and postselected states is denoted by ϕ and the parameter range is $g\ll\phi\ll 1$, the postselection process is primarily determined by ϕ, rather than by g. In other words, as ϕ increases from 0 into the weak-value region, the FI is continuously transferred from the postselection process to the successful-postselection photons.

Finally, we demonstrate that this transfer effect also exists in our scheme. From Eq. (10), disregarding the high-order terms of g, it is evident that ϕ_0 holds the same significance as $n\sin 2g$. To examine how ϕ_0 affects the postselection, we plot P_dQ_d, P_rQ_r, and F_p varying with ϕ_0 in Fig. 2, where the trend of FI transfer is clearly illustrated. It can be seen that P_dQ_d can reach the maximum scale $4n^2+4n$, with the peak corresponding to the horizontal coordinate $\phi_0=\pi-n\sin 2g-2g$. (The calculation here is straightforward because F_p decreases to 0 at the peak value of P_dQ_d. We simply need to solve for $F_p=0$.) Therefore, we conclude that during the transition of ϕ_0 from $\phi_0=\pi$ to $\phi_0=\pi-n\sin 2g-2g$, the FI gradually transfers from the postselection distribution (F_p) to the successful-postselection photons (P_dQ_d), resulting in the output photons $\sim n^2$ scaling. Next, we will further compare the merits and drawbacks of these two measurement scenarios from the perspective of dephasing noise.

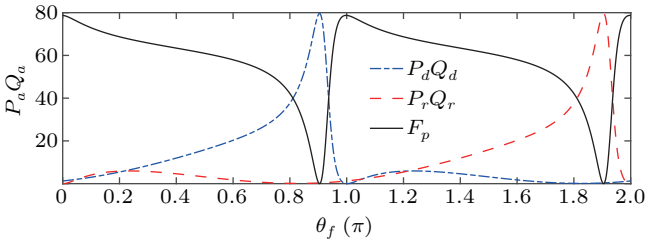


Fig. 2. Transfer of FI. P_dQ_d, P_rQ_r and F_p vary with the phase shift between the pre- and postselected state ϕ_0. In this plot, all P_dQ_d, P_rQ_r and F_p can achieve the maximum value of $4\bar{n}^2+4\bar{n}$. $F_{\rm tot}$is the sum total of the FI contained at different stages of the preselection–coupling–postselection process. P_dQ_d is the QFI of successful postselection photons. P_rQ_r is the QFI of failed postselection photons. F_p is the FI of the distribution of postselection probability.

3.2. Effects of phase fluctuations

While the preceding analysis addresses an idealized Heisenberg-scale model, the inevitable inclusion of decoherence/dephasing noise fundamentally alters the scaling dynamics, precipitating a characteristic transition from Heisenberg scaling to standard quantum scaling. Furthermore, although the meter states are seemingly classical coherent states, phase fluctuations (or other dephasing noise) in measuring two-state systems operating at the Heisenberg limit can severely affect the scheme's measurement conclusions. The theoretical basis for these assertions can be referenced in Ref. [28].

Here, we consider a small phase fluctuation δ, which is a Gaussian random variable with zero mean and variance $\langle\delta^2\rangle$. This effect manifests directly on the measured parameter g and can be averaged over, $g\to g+\delta$. In Ref. [28], Jordan *et al.* proposed that the perturbation to the coherent state is effectively an n-independent phase shift of the coherent state under the small $g\sim 1/n$ condition; that is, the coherent state in the weak-coupling regime can be approximated as

$$\left|\alpha\,{\rm e}^{\pm{\rm i}g}\right\rangle\approx|\alpha\rangle\,{\rm e}^{\pm{\rm i}gn}+|\alpha_\perp(\pm g)\rangle, \quad (11)$$

where $|\alpha_\perp(\pm g)\rangle$ is orthogonal to $|\alpha\rangle$ in this condition. Similarly, Eq. (2) can be approximated as

$$\begin{aligned}\left|\Psi_j'\right\rangle\approx{}&(1/\sqrt{2})\left(|g\rangle\,{\rm e}^{-{\rm i}gn}+|e\rangle\,{\rm e}^{{\rm i}gn}\right)|\alpha\rangle,\\&+(1/\sqrt{2})\left(|g\rangle\,|\alpha_\perp(-g)\rangle+|e\rangle\,|\alpha_\perp(g)\rangle\right), \quad (12)\end{aligned}$$

where we set the initial phase shift $\phi_i=0$. This equation reveals two key findings. (a) In the large-n limit, weak coupling primarily induces rotation of the spin while causing negligible

disturbance to the coherent state — a phenomenon diverging fundamentally from classical weak measurement predictions. (b) The coherent state is separable within the Heisenberg scaling regime, allowing all quantum effects to be captured by the first half of the equation, $(1/\sqrt{2})\left(|g\rangle\, e^{-igh} + |e\rangle\, e^{igh}\right)$. Therefore, the density matrix component associated with the Heisenberg scaling regime can be decoupled,

$$\rho \approx \frac{1}{2}(|g\rangle\langle g| + |e\rangle\langle e| + e^{-2igh-2ig\delta}|g\rangle\langle e| + e^{2igh+2ig\delta}|e\rangle\langle g|). \tag{13}$$

Here, we provide necessary clarification regarding the approximation above. The second term in Eq. (12), $(1/\sqrt{2})(|g\rangle|\alpha_\perp(-g)\rangle + |e\rangle|\alpha_\perp(g)\rangle)$ — which captures the coherent state's response to weak coupling — has been entirely discarded. One may readily demonstrate that this term's FI equals $4n$ in Eq. (8). This term scales linearly with n, whereas the present work focuses on quantum contributions that scale with n^2. It is therefore justifiable to neglect the linear term on physical grounds. Moreover, the large-n limit is essential to this study: typical photon numbers exceed 10^2, under which condition $Q_j = 4n^2 + 4n \approx 4n^2$ holds. Taking the average over δ, the density matrix becomes

$$\rho' \approx \frac{1}{2}\left(|g\rangle\langle g| + |e\rangle\langle e| + e^{-2igh-2n^2\langle\delta^2\rangle}|g\rangle\langle e| + e^{2igh-2n^2\langle\delta^2\rangle}|e\rangle\langle g|\right). \tag{14}$$

Next, we investigate the influence of phase fluctuations by calculating the QFI. Defining L as the logarithmic derivative of the density matrix ρ' with respect to g, the corresponding QFI can be given by

$$F_{\rho'} = \mathrm{Tr}(\rho' L^2) = 4n^2 e^{-4n^2\langle\delta^2\rangle}. \tag{15}$$

As shown in Fig. 3, the scaling of FI with measurement samples n is compared between the ideal scenario ($\langle\delta^2\rangle = 0$) and a weakly perturbed phase fluctuation scenario ($\langle\delta^2\rangle = 0.001$). Remarkably, even infinitesimal dephasing noise triggers a superlinear decay of FI, thereby exposing the extreme fragility of quantum-enhanced metrology against decoherence.

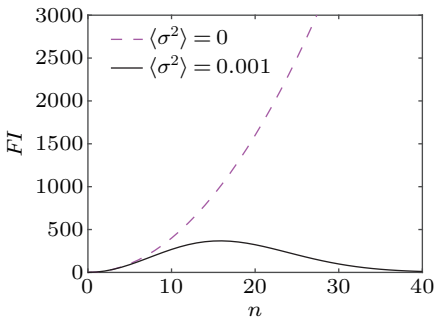


Fig. 3. The total QFI is highly sensitive to phase fluctuations. The curves of $F_{\rho'}$ versus n under both ideal conditions ($\langle\delta^2\rangle = 0$) and with a small phase fluctuation considered ($\langle\delta^2\rangle = 0.001$). $\langle\delta^2\rangle$ is the variance of phase fluctuation.

3.3. Robustness advantage of P_dQ_d measurement

In Subsection 3.2, we analyzed the dephasing noise of the initial joint states. To uncover the mechanism of dephasing evolution in the final detected states, we must examine the role of postselection. Here, we apply the postselected states $|\psi_f\rangle = (1/\sqrt{2})(|g\rangle + e^{i\phi_f}|e\rangle)$ to the density matrix ρ',

$$\rho'_f = |\psi_f\rangle\langle\psi_f|\rho'|\psi_f\rangle\langle\psi_f| = P'_d|\psi_f\rangle\langle\psi_f|, \tag{16}$$

where P'_d represents a specific probability and its mathematical expression is

$$P'_d = \frac{1 + e^{-2n^2\langle\delta^2\rangle}\cos(n\sin 2g + \phi_0)}{2}. \tag{17}$$

Notably, P'_d in this context embodies the HS probabilistic behavior of the protocol, distinct from the physical meaning of the actual postselection probability P_d, which corresponds to the experimentally measurable probability distribution. Since the postselected state $|\psi_f\rangle$ is independent of g (its derivative with respect to g vanishes), the QFI $F_{\rho'_f}$ of ρ'_f is fully captured by the FI of the probability P'_d,

$$F_{\rho'_f} = \mathrm{Tr}(\rho'_f L^2) = \frac{1}{P'_d}\left(\frac{dP'_d}{dg}\right)^2 + \frac{1}{1-P'_d}\left(\frac{d(1-P'_d)}{dg}\right)^2 = \frac{4n^2 e^{-4n^2\langle\delta^2\rangle}\sin^2(2gn+\phi_0)}{1 - e^{-4n^2\langle\delta^2\rangle}\cos^2(2gn+\phi_0)}. \tag{18}$$

In Subsection 3.1, we demonstrate that when $\phi_0 = \pi$, the total FI is concentrated in the distribution of postselection probability, whereas when $\phi_0 = \pi - n\sin 2g - 2g$, the total FI is entirely transferred to the output term P_dQ_d. Therefore, to compare the robustness of probability-distribution measurements and P_dQ_d measurements, one need only compare the total FI $F_{\rho'_f}$ at $\phi_0 = \pi$ and $\phi_0 = \pi - n\sin 2g - 2g$. As shown in Fig. 4(a), we plot $F_{\rho'}$ and $F_{\rho'_f}(\phi_0 = \pi)$ varying with $\langle\delta^2\rangle$. We find that the postselection-probability distribution measurement protocols exhibit heightened susceptibility to dephasing noise. To quantify this contrast, as shown in Fig. 4(b), we also focus on the trend of $F_{\rho'_f}(\phi_0 = \pi - n\sin 2g - 2g)$ where the total FI is concentrated in the output state. $F_{\rho'_f}(\phi_0 = \pi - n\sin 2g - 2g)$ almost overlaps with $F_{\rho'}$, which indicates that $F_{\rho'_f}(\phi_0 = \pi - n\sin 2g - 2g)$ is less affected by dephasing and thus has higher robustness than $F_{\rho'_f}(\phi_0 = \pi)$. To intuitively demonstrate the effect of postselection on robustness, we define the ratio of $F_{\rho'_f}$ to $F_{\rho'}$ as R, whose expression is

$$R = \frac{F_{\rho'_f}}{F_{\rho'}} = \frac{\sin^2(2gn+\phi_0)}{1 - e^{-4n^2\langle\delta^2\rangle}\cos^2(2gn+\phi_0)}. \tag{19}$$

R takes values between 0 and 1, where a larger R indicates stronger robustness of the measurement system. In Fig. 4(c), we visually demonstrate the variation trend of R, which provides a robustness advantage criterion for output-state measurements.

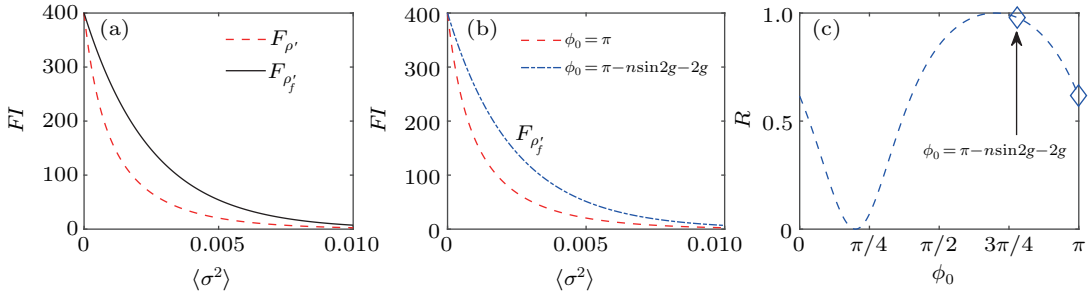


Fig. 4. Robustness analysis under different measurement scenarios. Panel (a) corresponds to the case of $F_{\rho'}$ and $F_{\rho'_f}(\phi_0=\pi)$ varying with $\langle\delta^2\rangle$, respectively, where $g=0.01\pi$ and $n=10$. Panel (b) compares the curves of $F_{\rho'_f}$ versus $\langle\delta^2\rangle$ for the cases of $\phi_0=\pi$ and $\phi_0=\pi-n\sin 2g-2g$. In panel (c), R is defined as the ratio of $F_{\rho'_f}$ to $F_{\rho'}$, and the plot displays the dependence of R on ϕ_0 over a full cycle. $\langle\delta^2\rangle$ is the variance of phase fluctuations. g is the coupling parameter.

4. Power-recycling

In Section 3, we demonstrate the robustness advantage of P_dQ_d measurements. However, weak measurement discards most photons during the postselection process, making it challenging for its signal-to-noise ratio to surpass that of conventional measurement methods. A solution to this limitation lies in the power-recycling technique, which essentially leverages the redistribution and concentration of FI. It transforms failed-postselection photons, which carry low information, into successful-postselection light with high information through a resonant cavity. Theoretically, it can enhance the FI of the outgoing photons by a factor of $1/\chi$, where χ is proportional to $\sqrt{P_d}$.[24,44] There is no doubt that this enhancement also applies to the coherent meter state here. However, during this photon transfer process, the postselection distribution changes. We will demonstrate that this change is also beneficial.

4.1. Power-recycling can benefit the distribution of postselection

Power-recycling technology involves inserting a partially transmitting mirror (PTM) with reflection and transmission coefficients r and p, respectively ($r^2+p^2=1$). Meanwhile, the postselection can be regarded as a specialized partially transmitting mirror, since it allows a small portion of photons to reach the detector, while the majority are reflected back to the PTM. Here, we assume the reflection coefficient of the postselection is r_m, which satisfies $r_m=\langle\psi_i|U|\psi_i\rangle=\sqrt{P_r}$. Thus, the corresponding transmission coefficient p_m can be given by $p_m=\sqrt{1-r_m}$. Considering an initial amplitude E_0 incident into the system, the amplitudes of reflected and transmitted light become $E_{rm}=r_mE_0$ and $E_{rt}=p_mE_0$, respectively, where we neglect optical loss. Therefore, the light inside the cavity and reflected back to the laser are, respectively,

$$\begin{aligned} E_{\rm c} &= p\left[1+rr_m{\rm e}^{{\rm i}\theta}+\left(rr_m{\rm e}^{{\rm i}\theta}\right)^2+\cdots\right]E_0 \\ &= \frac{p}{1-rr_m{\rm e}^{{\rm i}\theta}}E_0, \end{aligned} \tag{20}$$

$$E_{\rm b} = \left(-r+\frac{p^2r_m{\rm e}^{{\rm i}\theta}}{1-rr_m{\rm e}^{{\rm i}\theta}}\right)E_0, \tag{21}$$

where θ is the single-pass phase addition. For a resonant cavity, ${\rm e}^{{\rm i}\theta}\approx 1$, and the gain factor of amplitude is $E_{\rm cav}/E_0=p/(1-rr_m)$. As shown in Fig. 5, this leads to the successful-postselection probability changing from P_d to $P_{\rm c}$,

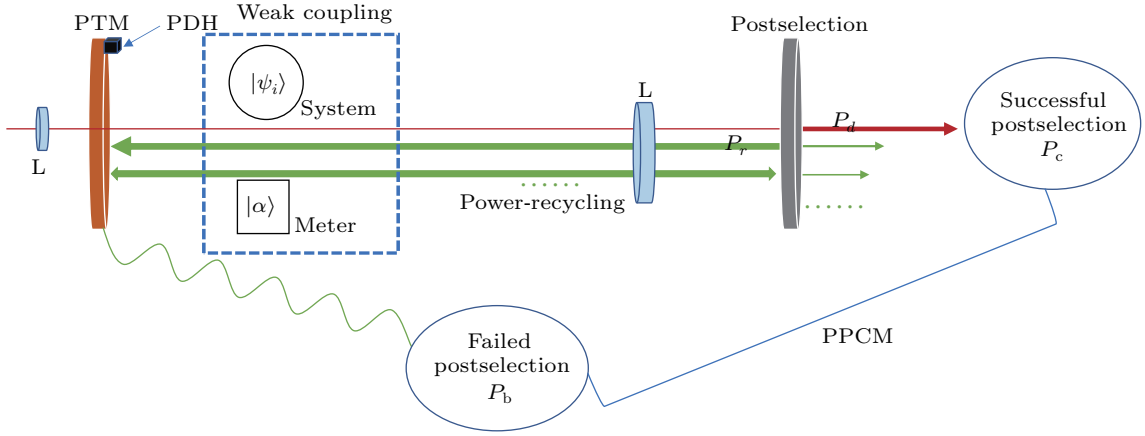


Fig. 5. Sketch of the power-recycled WVA-based metrology. The initial system state $|\psi_i\rangle$ is coupled to the meter state $|\alpha\rangle$. The partially transmitting mirror and the postselection system together constitute a power-recycling cavity. During the first pass through the postselection stage, a fraction P_d of photons is successfully postselected, while the remaining fraction P_r is failed postselected and reflected back toward the laser. After multiple cycles, both the successfully postselected photons with probability $P_{\rm c}$ and the failed postselected photons with probability $P_{\rm b}$ are detected via projective photon-counting measurement. PDH: the Pound–Drever–Hall technique, L: lens.

$$P_{\rm c} = \left(\frac{p}{1-r\sqrt{P_r}}\right)^2 P_d. \tag{22}$$

Note that the probability $P_{\rm c}$ critically incorporates the cavity-induced multi-interactions between the probe and the system. Similarly, the probability of failed postselection photons can be expressed as the square of the unnormalized amplitude of the light reflected back toward the laser

$$P_{\rm b} = \left(-r + \frac{p^2\sqrt{P_r}}{1-r\sqrt{P_r}}\right)^2. \tag{23}$$

By substituting the distribution of $\{P_{\rm c}, P_{\rm b}\}$ into Eq. (5), we can obtain the FI of postselection process modified by power-recycling

$$F_{\rm pow} = \frac{1}{P_{\rm c}}\left(\frac{{\rm d}P_{\rm c}}{{\rm d}g}\right)^2 + \frac{1}{P_{\rm b}}\left(\frac{{\rm d}P_{\rm b}}{{\rm d}g}\right)^2. \tag{24}$$

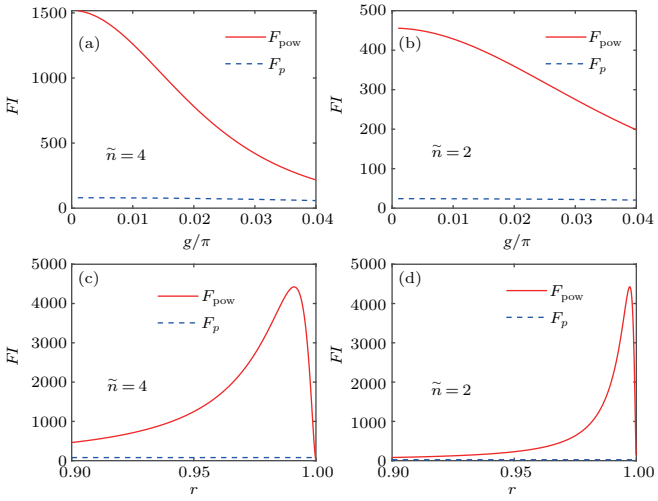


Fig. 6. Comparison of postselection in power-recycling and standard WVA schemes. Panels (a) and (b) correspond to the case of $F_{\rm pow}$ and F_p varying with g under $\bar{n}=4$ and 2, respectively, where $r=0.9$. In panels (c) and (d), we assume $g=0.01\pi$ and plot $F_{\rm pow}$ and F_p varying with r under $\bar{n}=4$ and 2, respectively. $F_{\rm pow}$ and F_p are the FI of the postselection process of power-recycling and standard schemes, respectively. g is the coupling parameter. r is the reflection coefficient of mirror.

To determine whether power-recycling affects the distribution of postselection, we first choose the optimal parameter $\phi=\pi$, which corresponds to the maximum F_p. Additionally, we assume $\sin g \approx g$ and neglect high-order terms of g ($g \ll 1$), thus simplifying $F_{\rm pow}$ to

$$F_{\rm pow} \approx n^2 B^2 \left[1 + \frac{(\cos ng - r)^2}{(1-r^2)\sin^2 ng}\right], \tag{25}$$

where

$$B = \frac{(1-r^2)(\sin 2ng + 2g\cos 2ng)}{(r\cos ng - 1)^2 \cos ng}. \tag{26}$$

It is evident that the power-recycled distribution of postselection can also achieve quantum precision ($\sim n^2$). To visualize this, as shown in Fig. 6, we plot the curves of $F_{\rm pow}$ (red solid line) and F_p (blue dashed line), where $F_{\rm pow}$ exhibits a broad-range enhancement. This implies that probability distribution $\{P_{\rm c}, P_{\rm b}\}$ contains significantly more FI than probability distribution $\{P_d, P_r\}$.

In addition, to analyze the source of the improvement in FI, we divide $F_{\rm tot}$ into two parts,

$$F_{\rm tot} = F_{\rm c} + F_{\rm b}, \tag{27}$$

where $F_{\rm c}$ is the contribution from the successful postselection part and $F_{\rm b}$ is the contribution from the failed postselection part. As shown in Fig. 7, we compare the trends of change in FI and postselection probabilities. We obtain two similar trends, but the magnitudes of these trends differ significantly. The conclusions are as follows. (i) The successful postselection part has a larger information-to-probability ratio than the failed postselection part. (ii) The power-recycling cavity transfers photons from the failed postselection part to the successful postselection part, thereby increasing the FI of postselection.

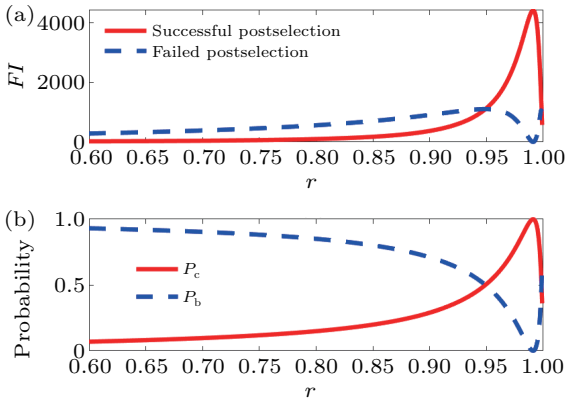


Fig. 7. The origin of the benefits of postselection induced by power-recycling. (a) The FI of successful and failed postselection parts varying with r under $\bar{n}=4$ and $g=0.01\pi$. (b) The trend of successful and failed postselection probabilities. $F_{\rm pow}$ and F_p are the FI of the postselection process of power-recycling and standard schemes, respectively. g is the coupling parameter. r is the reflection coefficient of mirror.

4.2. Experimental feasibility

Although this approach significantly enhances the FI of the distribution of postselection probability, its experimental implementation faces a major challenge: environmental noise. Here, we categorize this noise into two distinct types.

The first is noise independent of the recycling cavity — inherent to standard experimental configurations and also unavoidable in recycling-enhanced setups. This category comprises a combination of quantum and technical noise, and its model varies significantly across different measurement systems. Several methods are available to suppress such noise, particularly through techniques such as quantum error correction.[58,59] Fortunately, in photonic crystal fiber systems, a nearly optimal HS precision has been demonstrated for measuring single-photon Kerr nonlinearity.[60] Chen *et al.* have successfully implemented a weak measurement scheme with

HS precision in this system.[56] Thus, a recycling-enhanced verification protocol based on this system is feasible.

The second type arises specifically from the recycling cavity. This noise is predominantly technical in origin and typically includes vibrations, cavity power loss, and walk-off effects. Generally, the length of the resonant cavity is unstable and varies over time due to mechanical vibrations, thermal fluctuations, and pressure, among other factors. Wang *et al.* successfully stabilized the cavity length using the Pound–Drever–Hall (PDH) locking technique.[46] Therefore, the PDH system can also be employed to suppress vibrations in this power-recycling cavity. Cavity power loss — commonly characterized by the parameter γ denoting single-pass power loss — is generally unavoidable owing to imperfections inherent in the optical assembly. This makes the distribution of postselection probability as to

$$P_{\rm c}' = \left[\frac{p}{1-r\sqrt{(1-\gamma)P_r}}\right]^2 P_d,$$
$$P_{\rm b}' = \left[-r+\frac{p^2\sqrt{P_r}}{1-r\sqrt{(1-\gamma)P_r}}\right]^2. \tag{28}$$

The value of γ generally ranges from 0.1 to 0.3, depending on the specific optical system. Furthermore, the recycling beam tends to diminish in signal strength after multiple round trips, a phenomenon referred to as the walk-off effect. Although this effect is particularly challenging to eliminate in probability measurement systems, studies have shown that its impact can be significantly suppressed in noisy systems. By choosing appropriate optical design parameters (e.g., the partially transmitting mirror), its influence can approximately be neglected.[49]

5. Conclusion

In summary, we have considered the postselected metrology model proposed by Zhang *et al.*[27] and have analyzed the effect of FI transfer within it. We have drawn two key conclusions. (1) In addition to the postselection probability distribution measurement proposed by Zhang *et al.*, output-state measurements can also achieve Heisenberg-scale precision while exhibiting greater robustness against phase-dephasing noise. (2) Beyond its conventional role in improving the signal-to-noise ratio of successful output states, the power-recycling technique also positively modifies the distribution of postselection probability. These findings represent a direct optimization of the scheme introduced by Zhang *et al.* and, more fundamentally, highlight that weak measurements — particularly the postselection process — still harbor uncharted effects that are worthy of further exploration.

This FI transfer effect originates from postselection, and therefore it theoretically manifests in all postselection-related measurements. However, we do not analyze the connection between cyclic protocol and dephasing noise, since our noise model employs an 'unphysical' postselection probability, whereas cyclic methods typically directly amplify real postselection probabilities. Subsequent studies could therefore address noise model refinements for various improved weak measurement schemes.

Acknowledgments

Project supported by the Fundamental Research Funds for the Central Universities (Grant No. XJ2026003001) and the National Natural Science Foundation of China (Grant Nos. U25D8007, 61875067, and 12274164).

References

[1] Aharonov Y, Albert D Z and Vaidman L 1988 *Phys. Rev. Lett.* **60** 1351
[2] Steinberg A M 2010 *Nature* **463** 890
[3] Hosten O and Kwiat P 2008 *Science* **319** 787
[4] Zhou X, Xiao Z, Luo H and Wen S 2012 *Phys. Rev. A* **85** 043809
[5] Gorodetski Y, Bliokh K Y, Stein B, Genet C, Shitrit N, Kleiner V, Hasman E and Ebbesen T W 2012 *Phys. Rev. Lett.* **109** 013901
[6] Dixon P B, Starling D J, Jordan A N and Howell J C 2009 *Phys. Rev. Lett.* **102** 173601
[7] Starling D J, Dixon P B, Jordan A N and Howell J C 2009 *Phys. Rev. A* **80** 041803
[8] Starling D J, Dixon P B, Jordan A N and Howell J C 2010 *Phys. Rev. A* **82** 063822
[9] Xu X Y, Kedem Y, Sun K, Vaidman L, Li C F and Guo G C 2013 *Phys. Rev. Lett.* **111** 033604
[10] Viza G I, Martínez-Rincón J, Howland G A, Frostig H, Shomroni I, Dayan B and Howell J C 2013 *Opt. Lett.* **38** 2949
[11] Santana O J S, Carvalho S A, Leo S D and de Araujo L E E 2016 *Opt. Lett.* **41** 3884
[12] Egan P and Stone J A 2012 *Opt. Lett.* **37** 4991
[13] Li H, Huang J Z, Yu Y, Li Y, Fang C and Zeng G 2018 *Appl. Phys. Lett.* **112** 231901
[14] Magaña Loaiza O S, Mirhosseini M, Rodenburg B and Boyd R W 2014 *Phys. Rev. Lett.* **112** 200401
[15] de Lima Bernardo B, Azevedo S and Rosas A 2014 *Phys. Lett. A* **378** 2029
[16] Fang S Z, Tan H T, Li G X and Wu Q L 2021 *Appl. Opt.* **60** 4335
[17] Qiu X, Xie L, Liu X, Luo L, Li Z, Zhang Z and Du J 2017 *Appl. Phys. Lett.* **110** 071105
[18] Bai X, Liu Y, Tang L, Zang Q, Li J, Lu W, Shi H, Sun X and Lu Y 2020 *Opt. Express* **28** 15284
[19] Qu W, Jin S, Sun J, Jiang L, Wen J and Xiao Y 2020 *Nat. Commun.* **11** 1752
[20] Lundeen J S and Steinberg A M 2009 *Phys. Rev. Lett.* **102** 020404
[21] Huang J H, Jordan K M, Dada A C, Hu X Y and Lundeen J S 2025 *Phys. Rev. Lett.* **134** 080802
[22] Nishizawa A, Nakamura K and Fujimoto M K 2012 *Phys. Rev. A* **85** 062108
[23] Kedem Y 2012 *Phys. Rev. A* **85** 060102
[24] Jordan A N, Martínez-Rincón J and Howell J C 2014 *Phys. Rev. X* **4** 011031
[25] Tanaka S and Yamamoto N 2013 *Phys. Rev. A* **88** 042116
[26] Feizpour A, Xing X and Steinberg A M 2011 *Phys. Rev. Lett.* **107** 133603
[27] Zhang L, Datta A and Walmsley I A 2015 *Phys. Rev. Lett.* **114** 210801
[28] Jordan A N, Tollaksen J, Troupe J E, Dressel J and Aharonov Y 2015 *Quantum Stud. Math. Found.* **2** 5
[29] Ferrie C and Combes J 2014 *Phys. Rev. Lett.* **112** 040406
[30] Liu Y, Qin L and Li X Q 2022 *Phys. Rev. A* **106** 022619
[31] Ren J, Qin L, Feng W and Li X Q 2020 *Phys. Rev. A* **102** 042601
[32] Dressel J 2015 *Phys. Rev. A* **91** 032116
[33] Knee G C and Gauger E M 2014 *Phys. Rev. X* **4** 011032

[34] Alves G B, Escher B M, de Matos Filho R L, Zagury N and Davidovich L 2015 *Phys. Rev. A* **91** 062107
[35] Sinclair J, Hallaji M, Steinberg A M, Tollaksen J and Jordan A N 2017 *Phys. Rev. A* **96** 052128
[36] Harris J, Boyd R W and Lundeen J S 2017 *Phys. Rev. Lett.* **118** 070802
[37] Xu L, Liu Z, Datta A, Knee G C, Lundeen J S, Lu Y Q and Zhang L 2020 *Phys. Rev. Lett.* **125** 080501
[38] Brunner N and Simon C 2010 *Phys. Rev. Lett.* **105** 010405
[39] Dressel J, Malik M, Miatto F M, Jordan A N and Boyd R W 2014 *Rev. Mod. Phys.* **86** 307
[40] Liu J, Yang Q, Shou Y, Chen S, Shu W, Chen G, Wen S and Luo H 2024 *Phys. Rev. Lett.* **132** 043601
[41] Pang S and Brun T A 2015 *Phys. Rev. A* **92** 012120
[42] Arvidsson-Shukur D R M, Yunger Halpern N, Lepage H V, Lasek A A, Barnes C H W and Lloyd S 2020 *Nat. Commun.* **11** 3775
[43] Zhang M, Zhang J, Su W, Yang X, Wu C, Xie Y, Wu W and Chen P 2023 *Chin. Phys. Lett.* **40** 040301
[44] Lyons K, Dressel J, Jordan A N, Howell J C and Kwiat P G 2015 *Phys. Rev. Lett.* **114** 170801
[45] Dressel J, Lyons K, Jordan A N, Graham T M and Kwiat P G 2013 *Phys. Rev. A* **88** 023821
[46] Wang Y T, Tang J S, Hu G, Wang J, Yu S, Zhou Z Q, Cheng Z D, Xu J S, Fang S Z, Wu Q L, Li C F and Guo G C 2016 *Phys. Rev. Lett.* **117** 230801
[47] Fang S Z, Zhu L L, Jin R B, Tan H T, Li G X and Wu Q L 2020 *Opt. Commun.* **460** 125117
[48] Krafczyk C, Jordan A N, Goggin M E and Kwiat P G 2021 *Phys. Rev. Lett.* **126** 220801
[49] Zhong Z R, Tan W J, Chen Y and Wu Q L 2023 *Phys. Rev. A* **108** 032608
[50] Zhong Z R, Chen Y, Tan W J, Hu X M and Wu Q L 2024 *Phys. Rev. A* **109** 042602
[51] Strübi G and Bruder C 2013 *Phys. Rev. Lett.* **110** 083605
[52] Pang S, Dressel J and Brun T A 2014 *Phys. Rev. Lett.* **113** 030401
[53] Pang S and Brun T A 2015 *Phys. Rev. Lett.* **115** 120401
[54] Chen J S, Liu B H, Hu M J, Hu X M, Li C F, Guo G C and Zhang Y S 2019 *Phys. Rev. A* **99** 032120
[55] Kim Y, Yoo S Y and Kim Y H 2022 *Phys. Rev. Lett.* **128** 040503
[56] Chen G, Zhang L, Zhang W H, Peng X X, Xu L, Liu Z D, Xu X Y, Tang J S, Sun Y N, He D Y, Xu J S, Zhou Z Q, Li C F and Guo G C 2018 *Phys. Rev. Lett.* **121** 060506
[57] Chen G, Aharon N, Sun Y N, Zhang Z H, Zhang W H, He D Y, Tang J S, Xu X Y, Kedem Y, Li C F and Guo G C 2018 *Nat. Commun.* **9** 93
[58] Li P X, Xu L P, Hu G T and Gao W L 2025 *Chin. Phys. B* **34** 070303
[59] Hong H Y, Lu X J and Kuang S 2023 *Chin. Phys. B* **32** 040603
[60] Russell P 2003 *Science* **299** 358